

Enhancement of nuclear spin coherence times by driving dynamic nuclear polarization at defect centers in solids

Gargee Sharma¹, Torsten Gaebel², Ewa Rej², David J. Reilly², Sophia E. Economou¹, and Edwin Barnes¹

¹*Department of Physics, Virginia Tech, Blacksburg, VA 24061, U.S.A*

²*ARC Centre of Excellence for Engineered Quantum Systems, School of Physics, University of Sydney, Sydney, New South Wales 2006, Australia*

The hyperpolarization of nuclear spins can enable powerful imaging and sensing techniques provided the hyperpolarization is sufficiently long-lived. Recent experiments on nanodiamond ¹³C nuclear spins demonstrate that relaxation times can be extended by three orders of magnitude by building up dynamic nuclear polarization (DNP) through the driving of electron-nuclear flip-flop processes at defect centers. This finding raises the question of whether the nuclear spin coherence times are also impacted by this hyperpolarization process. Here, we theoretically examine the effect of DNP on the nuclear spin coherence times as a function of the hyperpolarization drive time. We do this by developing a microscopic theory of DNP in a nuclear spin ensemble coupled to microwave-driven defect centers in solids and subject to spin diffusion mediated by internuclear dipolar interactions. We find that, similarly to relaxation times, the nuclear spin coherence times can be increased substantially by a few orders of magnitude depending on the driving time. Our theoretical model and results will be useful for current and future experiments on enhancing nuclear spin coherence times via DNP.

I. INTRODUCTION

The loss of quantum coherence for nuclear spins remains an important problem in diverse fields such as high resolution magnetic resonance imaging and quantum computation. While on one hand decoherence can lead to broadening of the NMR peak linewidth, it also can lead to errors in the processing of quantum information in systems where nuclear spin states serve as qubits or quantum memories¹⁻¹⁵. Decoherence results from the interaction of the spin with various environmental degrees of freedom, with the most prominent channel being the interaction of the nuclear spin with other neighboring entities such as another nucleus via the dipole-dipole interaction or electron spin centers via the hyperfine interaction. Nuclear spin-flips resulting from these interactions can induce the loss of information stored in spins and lead to decoherence. Since electron-nuclear hyperfine interaction remains an important factor to consider at low temperatures, quantum decoherence of nuclear spins also can lead to loss of coherence of electron spins in systems where the electron coherence time is important. Therefore it is of fundamental and technological interest to control and manipulate the underlying nuclear spin degrees of freedom in order to extend the coherence time of nuclear spins.

In addition to being a source of decoherence, the electron-nuclear hyperfine interaction can also be used to manipulate the state of the nuclear spin ensemble and in particular to create dynamic nuclear polarization (DNP)¹⁶. DNP refers to the generation of a significant nuclear spin polarization through dynamic processes such as driving an electronic system with an external field and subsequent spin polarization transfer from electrons to the nuclei. This technique was initially suggested by A. Overhauser¹⁷ in 1953, and is currently a powerful method that is applicable to a wide variety of physical systems and applications. In solids DNP can be achieved by driving the system with optical fields or with microwave fields oscillating close to the electron Larmor frequency, and as a result the large spin polarization of the electrons is transferred

to nuclei via a process known as the solid effect¹⁸⁻²⁹. The polarization created in the nuclear spin ensemble via driven DNP processes will gradually relax and decohere due to internuclear dipolar interactions and other environmental factors.

Let us consider a simple two level system which consists of a single spin in the presence of an external magnetic field $\mathbf{B} = (B_{\perp}^x(t), B_{\perp}^y(t), B_{\parallel})$ in a perfectly isolated environment. The spin Hamiltonian is given by $H = -\boldsymbol{\mu} \cdot \mathbf{B}$, where $\boldsymbol{\mu} = -g\mu_n\boldsymbol{\sigma}$, and $\boldsymbol{\sigma}$ is the vector of Pauli spin matrices. The spin dynamics under this Hamiltonian is governed by the von Neumann equation for the density matrix $\dot{\rho} = -i[H, \rho]$. In the interaction frame, the equations of motion for the components of the density matrix can be written as $i\dot{\rho}_{\uparrow\uparrow} = \Omega(\rho_{\uparrow\downarrow}^* - \rho_{\uparrow\downarrow})$, and $i\dot{\rho}_{\uparrow\downarrow} = \delta\rho_{\uparrow\downarrow} + \Omega(\rho_{\downarrow\downarrow} - \rho_{\uparrow\uparrow})$ where δ is the detuning frequency of the applied transverse rotating field, Ω is the corresponding Rabi frequency, and the arrow represents the direction of the spin. The time evolution of this spin system is perfectly unitary since we have assumed the spin is perfectly isolated from its environment. Consequently in this ideal situation, the coherence time is infinite as the phase information is always maintained. However as we discussed above, coupling to various environmental degrees of freedom needs to be accounted for in the Hamiltonian, which leads to loss of spin coherence over time. Due to the complicated and many-particle nature of this problem, which involves several microscopic environmental parameters, a simpler phenomenological approach to this problem is to add decay terms in the equations i.e. $i\dot{\rho}_{\uparrow\uparrow} = \Omega(\rho_{\uparrow\downarrow}^* - \rho_{\uparrow\downarrow}) - i\rho_{\uparrow\uparrow}/T_1$, and $i\dot{\rho}_{\uparrow\downarrow} = \delta\rho_{\uparrow\downarrow} + \Omega(\rho_{\downarrow\downarrow} - \rho_{\uparrow\uparrow}) - i\rho_{\uparrow\downarrow}/T_2$. This phenomenological approach successfully describes a variety of experiments^{30,31}. The parameters T_1 and T_2 characterize longitudinal and transverse relaxation respectively in the two level system and can be extracted from experimental measurements.

It is the transverse dephasing time T_2 which characterizes how long a quantum state remains coherent. In the fields of magnetic resonance imaging and quantum computation, pulse sequence techniques have been developed as a method to reduce spin dephasing and thereby increase the T_2 coherence

time^{32–39}. Some well known examples of these include Hahn’s spin echo (single π pulse), the Carr-Purcell-Meiboom-Gill (CPMG) pulse sequence (multiple π pulses), and periodic dynamical decoupling (PDD). These control techniques extend coherence times by effectively decoupling the system from its environment.

In semiconductors, it has been shown that electron spin dephasing times (T_{2e}^*) can be extended by programming the nuclear spin ensemble as this effectively reduces the number of degrees of freedom and, consequently, the variance in effective fields sampled by an ensemble of experiments^{40–42}. DNP is also expected to enhance electron spin coherence times (T_{2e})⁴³, although this has yet to be demonstrated in experiment. Recent experiments have demonstrated an increase in the relaxation time of nanodiamond ^{13}C spins by dynamically polarizing the nuclear bath via microwave assisted DNP²⁸. The nuclear spin relaxation time has been observed to increase with the hyperpolarization time by 3 orders of magnitude. This raises the question of whether the nuclear spin coherence time is similarly impacted by this hyperpolarization process.

In this work we theoretically examine the effect of DNP on nuclear spin coherence and calculate T_2 as a function of the driving time. We start with a central spin model of an electron located at a paramagnetic site interacting with the surrounding nuclear bath via the hyperfine interaction. Driving this system at a microwave frequency close to the ESR frequency then induces a large DNP in the surrounding nuclear spin bath, which typically spreads out to a few nanometers around the electron site. Using Liouville’s equation, we then calculate the spatial distribution of the nuclear polarization around the electron site as a function of the driving time. The DNP induced effective magnetic field produced by polarization of the nuclear spins in the crystal however also undergoes its own dynamics due to the internuclear dipole-dipole coupling^{44,45}. These dynamics lead to local fluctuations in the nuclear spin field. Since the exact quantum mechanical treatment of this mechanism (which is a many-particle dipolar interaction) is quite complicated, in this work we treat the dynamical evolution of nuclear spins caused by such an interaction using a stochastic diffusion model for an effective nuclear spin field^{46,47}, which remains a valid approximation for the time scales considered in this work. Using an effective Gaussian model for the DNP solution, we then analytically calculate the nuclear spin-spin correlation function, which is crucial for the evaluation of the T_2 time. Finally, we calculate the T_2 coherence time and study its dependence under dynamical decoupling pulse sequences (like SE, CPMG) as a function of the driving time. We find that the nuclear T_2 coherence time substantially increases by a few orders of magnitude depending on the DNP drive time. We also apply our results to calculate the T_2 time of ^{13}C nuclear spins for experimentally relevant parameters. Our theoretical model and results will be useful for current and upcoming experiments on enhancing the coherence time of nuclear spins via DNP.

This paper is organized as follows: In Sec II we discuss dynamic nuclear polarization in solids and obtain an exact numerical solution for the spatial distribution of nuclear polarization for a microwave driven DNP process enabled by

electron-nuclear hyperfine interaction. In Sec III we discuss the problem of diffusion of the spin polarization into the bulk of the sample within the framework of a stochastic model, and also calculate the two point correlation function. In Sec IV we evaluate the nuclear spin coherence time as a function of the polarization time. We conclude in Sec V.

II. DYNAMIC NUCLEAR POLARIZATION

In this section we will discuss DNP in solids and obtain an exact numerical solution for the spatial distribution of nuclear polarization for a microwave driven DNP process enabled by electron-nuclear hyperfine interaction. Since the hyperfine interaction involves a spin-flip term, it can allow electron spin polarization to be transferred to the nuclei. This transfer of spin polarization can be accelerated by the application of microwave radiation operating at a suitable frequency close to the Larmor frequency of the electron. In Fig. 1 we present a schematic representation of polarization transfer via the DNP process considered in our model. The single electron center, which is usually located at a defect or a paramagnetic site, constitutes an ESR line at a frequency ω_{0s} under an external magnetic field. The nuclear spins in a radius of $r < a$ around the electron center are strongly coupled to the electron and do acquire a net polarization because they continually undergo flip-flops with the electron spin. The distance a can typically vary between 0.1nm-0.3nm⁴⁸. These spins are effectively isolated from the bulk nuclear spin diffusion by the strong electron-nuclear coupling, which shifts the resonances of the neighboring nuclei, and hence they interact weakly with the bulk^{48,49}. The nuclei outside this barrier that are within $a < r < b$ are directly polarized and relax via the DNP process and subsequent diffusion. Driving the system at a microwave frequency $\omega_m = \omega_{0s} - \omega_{0I}$ results in a spin polarization transfer between electron and nuclei. The distance b , which depends upon the transition probabilities of the hyperpolarization mechanisms and relaxation, can typically extend up to a few nanometers^{50,51}. The nuclear spin polarization is transferred further away to the bulk of the system for $b < r < c$ via the process of nuclear spin diffusion, which is mediated by dipole-dipole interaction between the nuclei.

To gain a more quantitative understanding of the DNP process in this scenario, let us begin by first considering the case of a single unpaired electron (at a paramagnetic site) in a solid located at the origin which is coupled to the surrounding nuclear bath in the presence of a magnetic field. The total Hamiltonian for this system is given by

$$H = H^e + H^n + H^{en} + H^{nn}, \quad (1)$$

where $H^e = \omega_{0s}S_z$ and $H^n = -\sum_i \omega_{0I}I_z^i$ are the Zeeman energies of the electron and the nuclei respectively in the presence of an external magnetic field. The summation i is over all the nuclei, which are assumed to be of the same species for simplicity. H^{en} is the hyperfine interaction between electron and nuclei, and H^{nn} is the dipole-dipole interaction between the nuclei. The hyperfine coupling between the elec-

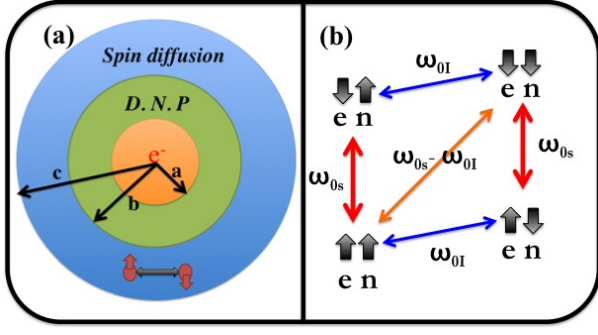


FIG. 1. (a) A schematic representation of polarization transfer via DNP. The electron center constitutes an ESR line at a frequency ω_{0s} . The nuclear spins in a radius of $r < a$ around the electron center are strongly polarized while the nuclei within $a < r < b$ participate in the DNP process. The spin polarization is transferred further away to $b < r < c$ via nuclear spin diffusion mediated by dipole-dipole interactions between the nuclei. In red is shown a possible nuclear process where there is a spin flip-flop between pairs of nuclei, leading to local fluctuations in the nuclear field. (b) The corresponding energy level diagram. The ESR line is at frequency ω_{0s} and the NMR line is at frequency ω_{0I} . Driving the system at a microwave frequency $\omega_m = \omega_{0s} - \omega_{0I}$ results in a spin polarization transfer between electron and nuclei (DNP).

tron and nuclei comprises an isotropic contact hyperfine interaction $\sim a_{iso} S \cdot I$ (which requires a non-zero overlap between the electron and nuclear wave functions and is therefore localized near the electron site), and the anisotropic interaction given by the dipolar coupling between the electron and nuclear magnetic moments. For our purposes we will only consider the dipolar coupling, retaining parts which are significant under the high magnetic field approximation³⁰. The Hamiltonian H^{en} (for a single electron-nucleus system) can then be written as

$$H^{en} = A_1 S_z I_z + A_2 S_z I_x, \quad (2)$$

where A_1 and A_2 are the secular and non-secular parts of the interaction respectively³⁰

$$A_1 = T(3 \cos^2 \theta - 1), \quad (3)$$

$$A_2 = 3T \sin \theta \cos \theta, \quad (4)$$

where $T = (\mu_0/4\pi r^3) \gamma_e \gamma_N \hbar^2$ is the bare hyperfine strength, r is the distance between the electron center and nuclear spin, θ is the polar angle, γ_e and γ_N are the electron and nuclear gyromagnetic ratios. Note that a non-zero A_2 facilitates the DNP process as we will see shortly. Diagonalizing the Hamiltonian $H_0 = H^e + H^n + H^{en}$ for a single electron-nucleus system we have

$$\tilde{H}_0 = \omega_{0s} S_z - \tilde{\omega}_{0I} I_z + A' S_z I_z, \quad (5)$$

where

$$\begin{aligned} \tilde{\omega}_{0I} &= \frac{\omega_{0I}}{2} (\cos \eta_- + \cos \eta_+) - \frac{A_1}{4} (\cos \eta_- - \cos \eta_+) \\ &\quad - \frac{A_2}{4} (\sin \eta_- - \sin \eta_+), \end{aligned} \quad (6)$$

$$\begin{aligned} A' &= -\omega_{0I} (\cos \eta_- - \cos \eta_+) + \frac{A_1}{2} (\cos \eta_- + \cos \eta_+) \\ &\quad + \frac{A_2}{2} (\sin \eta_- + \sin \eta_+), \end{aligned} \quad (7)$$

$$\tan \eta_{\mp} = \frac{A_2}{A_1 \mp 2\omega_{0I}}. \quad (8)$$

To study DNP in this system, we now introduce the microwave field $H_M = B_e S_x \cos(\omega_m t)$, which can drive the nuclear spin flip transitions for particular values of the drive frequency ω_m . In the diagonal basis of H_0 the microwave Hamiltonian (\tilde{H}_M) becomes⁵²

$$\begin{aligned} \tilde{H}_M &= B_e \cos(\omega_m t) (S_x \cos \delta - \frac{1}{2} (S_+ I_- + S_- I_+) \sin \delta \\ &\quad + \frac{1}{2} (S_+ I_+ + S_- I_-) \sin \delta), \end{aligned} \quad (9)$$

where $2\delta = \eta_- - \eta_+$. The $S_{\pm} I_{\pm}$ terms in the above Hamiltonian are the spin-flip terms. When $A_2 = 0$, these spin flip terms in \tilde{H}_M vanish, indicating the absence of any microwave driven nuclear polarization. Note that from Eq. 4, A_2 is generically non-zero except when $\theta = n\pi/2$, where $n = \{0, 1, 2, 3\}$. When $A_2 \neq 0$, either the $S_+ I_- + S_- I_+$ or the $S_+ I_+ + S_- I_-$ terms facilitate the transfer of nuclear polarization. In the interaction frame of H_0 , one can derive an effective Hamiltonian H_{eff} when the microwave frequency is tuned to drive either of the nuclear spin flip transitions. Specifically, when $\omega_m = \omega_{0s} - \omega_{0I}$ the double spin-flip term $S_+ I_+ + S_- I_-$ in \tilde{H}_M is selected and H_{eff} becomes

$$H_{\text{eff}} = \frac{B_e}{4} \sin \delta (S_+ I_+ + S_- I_-). \quad (10)$$

In the interaction frame of reference, microwave driven nuclear dynamics can then be described by the Liouville-von Neumann equation $\dot{\rho} = -i[H_{\text{eff}}, \rho] + L[\rho]$, where we can solve for the evolution of the density matrix ρ corresponding to the 4-component electron-nuclear spin system. The Lindblad operator $L[\rho]$ accounts for relaxation processes (like decay of the electron spin to the ground state), which gives a non-unitary evolution of the quantum system and consequently a steady state solution for $\rho(t)$ when $t \rightarrow \infty$. Specifically $L[\rho]$, which is the relaxation superoperator term, can be expressed as

$$L[\rho] = \sum_k \left(L_k \rho L_k^\dagger - \frac{1}{2} [L_k^\dagger L_k \rho + \rho L_k^\dagger L_k] \right), \quad (11)$$

where L_k are the Lindblad operators. The index k runs from 1 to 4, with the non-trivial elements of the Kraus operators being $\langle \uparrow\uparrow | L_1 | \downarrow\uparrow \rangle = \sqrt{\gamma_2}$, $\langle \uparrow\downarrow | L_2 | \downarrow\downarrow \rangle = \sqrt{\gamma_2}$, $\langle \uparrow\uparrow | L_3 | \downarrow\downarrow \rangle = \sqrt{\gamma_1}$, $\langle \uparrow\downarrow | L_4 | \downarrow\uparrow \rangle = \sqrt{\gamma_1}$, where the first (second) arrow indicates the direction of the electron (nuclear) spin. L_1 and L_2 describe processes conserving nuclear spin, while L_3 and L_4 describe (much slower) processes involving flipping of the nuclear spin as well. The Liouville-von Neumann equation can be solved analytically as $\tilde{\rho}(t) = S(t)\tilde{\rho}(0)$, where $\tilde{\rho}(t)$ is the density matrix $\rho(t)$ written as a single column vector, and the matrix $S(t)$ is $S(t) = e^{(\mathcal{H}+\mathcal{G})t}$, where $\mathcal{H} = i(H_{\text{eff}} \otimes I - I \otimes$

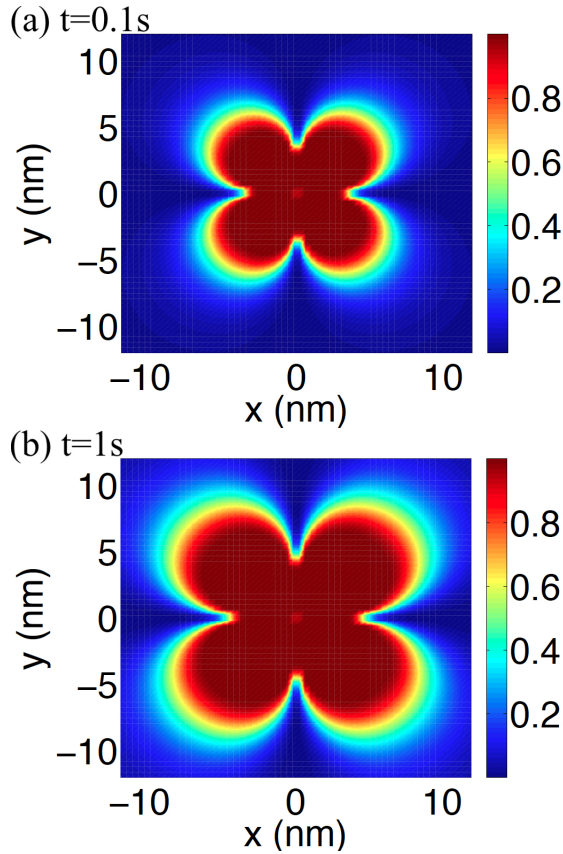


FIG. 2. Spatial profile $\langle P_z(r, \theta, t) \rangle$ of the microwave driven nuclear polarization around the electron center at the origin as obtained from the solution of the Liouville-von Neumann equation at various times. (a) At time $t = 0.1\text{s}$. (b) At time $t = 1\text{s}$. We use the parameters $\omega_{0s} = 10\mu\text{eV}$, $B_e = 0.1\mu\text{eV}$, $\omega_{0I} = 0.0004\omega_{0s}$. The relaxation parameters for the Lindblad operator used were $\gamma_1 = 1\mu\text{s}$, and $\gamma_2 = 1\text{s}$. Note that this so far does not account for nuclear diffusion (which is the subject of Sec III), but rather provides an initial condition to that problem.

$$H_{\text{eff}}, \mathcal{G} = \sum_m [L_m \otimes L_m - \frac{1}{2}I \otimes L_m^\dagger L_m - \frac{1}{2}L_m^\dagger L_m \otimes I].$$

Thus for an arbitrary initial condition $\rho(0)$, the density matrix $\rho(t)$ at a later time can be evaluated exactly.

Once we obtain the solution for $\rho(t)$, tracing over the nuclear degree of freedom then gives us the magnitude of induced nuclear polarization. The spatial profile (which arises from the spatial dependence of the hyperfine constants A_1 and A_2) of the induced nuclear polarization around the electron center can also be studied as a function of the microwave driving time by evaluating the mean value of nuclear polarization $\langle P_z(t, r, \theta) \rangle = \text{Tr}(P_z \rho(t, r, \theta))$ where the operator P_z is the nuclear spin operator I_z written in the rotating frame basis of H_0 .

In Fig. 2 we plot the spatial profile of the microwave driven nuclear polarization around the electron center at the origin as obtained from the solution of the Liouville-von Neumann equation at various times. Clearly the spread of DNP with increasing drive times is evident. Even though the spatial profile around the electron center is not isotropic, the schematic

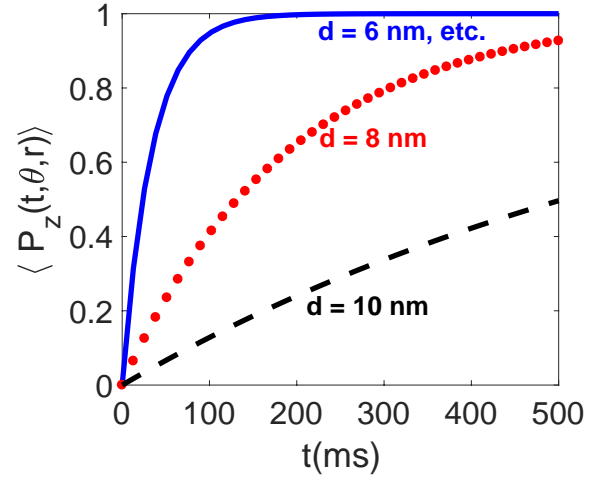


FIG. 3. Time evolution of DNP around the electron center at the origin as obtained from the solution of the Liouville-von Neumann equation at various distances from the origin. We use the parameters $\omega_{0s} = 10\mu\text{eV}$, $B_e = 0.1\mu\text{eV}$, $\omega_{0I} = 0.0004\omega_{0s}$, $\theta = \pi/4$. The relaxation parameters for the Lindblad operator used were $\gamma_2 = 1\mu\text{s}$, and $\gamma_1 = 1\text{s}$. Also note that this solution so far does not account for nuclear spectral diffusion (which is the subject of Sec III), but rather serves as its initial condition.

representation presented in Fig. 1 provides us with a good approximation to the problem. The DNP solution will be used as an initial condition for the problem of nuclear spin diffusion (which is the subject of Sec III). Fig. 3 shows the time evolution of DNP at various distances from the origin as obtained from the solution of the Liouville equation.

III. NUCLEAR SPIN DIFFUSION

We have so far focused on the problem of DNP in solids, which produces a large spin polarization of the nuclei around the paramagnetic electron center. In this section we will discuss the problem of diffusion of the spin polarization into the bulk of the sample. The large nuclear Overhauser field produced via DNP in the vicinity of this electron defect site dynamically evolves through mutual dipole-dipole coupling of the nuclei. This also causes temporal fluctuations of the nuclear spin field due to processes such as a pair of spin flips. Since the exact quantum mechanical treatment of this many-particle dipolar interaction is quite complicated, we will describe the dynamical evolution of the nuclear spin field with the following stochastic diffusion model⁴⁶

$$\frac{\partial I(\mathbf{x}, t)}{\partial t} = D \frac{\partial^2}{\partial \mathbf{x}^2} I(\mathbf{x}, t) + \zeta(\mathbf{x}, t). \quad (12)$$

In the above equation $I(\mathbf{x}, t)$ is the nuclear field, which on a coarse-grained scale encompasses several atomic sites, D is the isotropic diffusion constant, and $\zeta(\mathbf{x}, t)$ is an effective stochastic field which models the randomness associated with the nuclear spin flips. Following Ref. 46, we treat the field

$\zeta(\vec{x}, t)$ as behaving like white noise, which has the following correlation functions

$$\langle \zeta(\mathbf{x}, t) \rangle = 0, \quad (13)$$

$$\langle \zeta(\mathbf{x}, t) \zeta(\mathbf{y}, s) \rangle = \Gamma_0 \delta(\mathbf{x} - \mathbf{y}) \delta(t - s). \quad (14)$$

In the above equations, averaging is done over all possible noise realizations. The average noise is zero, and choosing $\Gamma_0 = -\eta D \partial^2 / \partial \mathbf{x}^2$ leads to the conservation of the order parameter⁵³ (which is the total nuclear spin polarization in the present case), in any possible noise realization. The parameter η determines the noise strength. It is convenient to switch to Fourier space, where Eq. 12 becomes

$$\frac{\partial}{\partial t} I(\mathbf{q}, t) = -Dq^2 I(\mathbf{q}, t) + \zeta(\mathbf{q}, t). \quad (15)$$

The above equation has the following general solution

$$I(\mathbf{q}, t) = I(\mathbf{q}, 0) e^{-Dq^2 t} + \int_0^t ds e^{-Dq^2(t-s)} \zeta(\mathbf{q}, s). \quad (16)$$

Fourier transforming Eq. 14 we find that the noise correlations in Fourier space take the following form

$$\langle \zeta(\mathbf{q}, t) \zeta(\mathbf{k}, s) \rangle = (2\pi)^3 \eta D q^2 \delta(\mathbf{q} + \mathbf{k}) \delta(t - s). \quad (17)$$

Note that the above correlation function vanishes for the zeroth ($\mathbf{q} = 0$) Fourier mode, implying a strict conservation of the total nuclear spin polarization. The spin-spin correlation function then becomes

$$\begin{aligned} \langle I(\mathbf{q}, t) I(\mathbf{k}, s) \rangle &= e^{-Dq^2(t+s)} \langle I(\mathbf{q}, 0) I(\mathbf{k}, 0) \rangle \\ &\quad - \frac{\eta}{2} (2\pi)^3 \delta(\mathbf{q} + \mathbf{k}) (e^{-Dq^2(t+s)} - e^{-Dq^2|t-s|}), \end{aligned} \quad (18)$$

which can be evaluated once the initial correlation function $\langle I(\mathbf{q}, 0) I(\mathbf{k}, 0) \rangle$ at time $t = 0$ is known. In the absence of any DNP or any other dynamic processes, this function can be drawn from a stationary equilibrium distribution, however in the present case this initial condition is determined by the solution of DNP (which has been treated in detail in Sec II). The exact functional form $I(\mathbf{x}, 0)$ of the spatial distribution of DNP (see Fig. 2) is not a simple mathematical function with a precise closed form. Hence to make our model analytically tractable for subsequent analysis, we will first assume the following simplified form for $I(\mathbf{x}, 0)$ centered around the defect site (at the origin):

$$I(\mathbf{x}, 0) = I_0 \exp(-\alpha^2(x^2 + y^2 + z^2)). \quad (19)$$

Note that the parameter α has a crucial dependence on the DNP driving time. Specifically, for longer driving times, the spread of the nuclear polarization around the origin should increase, and therefore α should decrease. For a fixed I_0 the total nuclear spin polarization (z -component) in the sample is $I_0 \pi^{3/2} \alpha^{-3}$, which again highlights the fact that the nuclear polarization increases with driving time. Since we have now

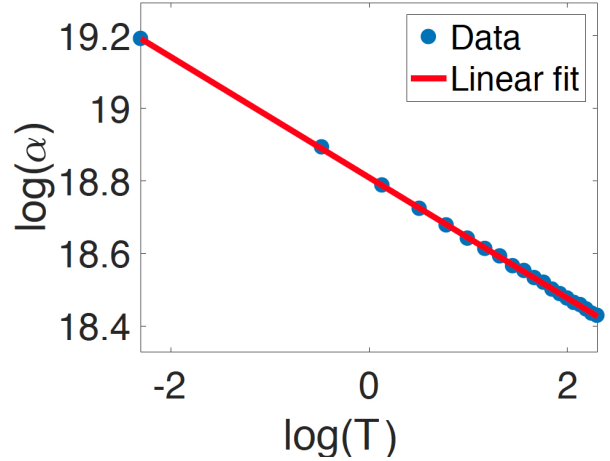


FIG. 4. Logarithm (natural) of the numerically evaluated α (in the units m^{-1}) as a function of the logarithm (natural) of the driving time T (in the units s) using the Gaussian approximation along a particular direction ($\theta = \pi/4$). The plot shows the data (in blue dots) for $\log(\alpha)$ as a function of $\log(T)$. The data shows a linear behavior shown in the red line (at least for the timescales we are concerned with), and thus can be extrapolated to obtain α for arbitrary driving times. The parameters chosen are the same as in Fig. 2. We find that for those parameters, $\log(\alpha(T)) = T^{a_1} + a_2$, with $a_1 = -0.16632$, and $a_2 = 18.8096$.

approximated the DNP distribution to be of Gaussian form involving the parameter α , we must numerically determine α as a function of driving time T using our exact DNP solution from Sec. II. We do this by calculating the full width at half maximum (FWHM) along a chosen direction from our actual DNP solution (see Fig. 2), and relating the calculated FWHM to the standard deviation of our Gaussian approximation, i.e., $\text{FWHM} = 2\sqrt{\ln 2}/\alpha$. Fig. 4 shows the plot of the numerically evaluated α as a function of driving time (T) using the Gaussian approximation. Since the plot of $\log(\alpha)$ vs. $\log(T)$ has a linear fit, one can easily obtain α for arbitrary driving times.

Fourier transforming Eq. 19, we have the initial condition

$$I(\mathbf{q}, 0) = \pi^{3/2} \frac{I_0}{\alpha^3} \exp(-(q_x^2 + q_y^2 + q_z^2)/4\alpha^2). \quad (20)$$

We can then calculate the correlation function at finite times using Eq. 18:

$$\begin{aligned} \langle I(\mathbf{q}, t) I(\mathbf{k}, s) \rangle &= \pi^3 \frac{I_0^2}{\alpha^6} e^{-(q^2 + k^2)/4\alpha^2 - Dq^2(t+s)} \\ &\quad - \frac{\eta}{2} (2\pi)^3 \delta(\mathbf{q} + \mathbf{k}) (e^{-Dq^2(t+s)} - e^{-Dq^2|t-s|}). \end{aligned} \quad (21)$$

Since the spatial and temporal distribution of the nuclear spin field is given by $I(\mathbf{x}, t)$, the effective magnetic field at any given nucleus in the sample is given by

$$\begin{aligned} B(t) &= \gamma_N \int d^3 \mathbf{x} n(\mathbf{x}) I(\mathbf{x}, t) \\ &= \gamma_N \int \frac{d^3 \mathbf{q}}{(2\pi)^3} n(\mathbf{q}) I(-\mathbf{q}, t), \end{aligned} \quad (22)$$

where $n(\mathbf{x})$ is the spatial nuclear density profile of the nucleus, and $n(\mathbf{q})$ is its Fourier transform. For a given single nucleus centered at $(x_0, 0, 0)$, we can approximate its spatial distribution to be a Gaussian i.e.

$$n(\mathbf{x}) = \left(\frac{\beta^2}{\pi}\right)^{3/2} \exp(-((x-x_0)^2 + y^2 + z^2)\beta^2), \quad (23)$$

$$n(\mathbf{q}) = \exp(-(q_x^2 + q_y^2 + q_z^2)/4\beta^2) \exp(-iq_x x_0). \quad (24)$$

The parameter β related to the spatial spread of the nucleus can be adjusted to represent a scenario close to the actual physical case such that $n(\mathbf{x})$ is close to a Dirac-delta function. To obtain physically relevant results, an ensemble averaging over many nuclear sites can be performed by varying the position of the center of the nucleus. For a particular angle θ the value of the parameter α can be calculated as described previously, and for that chosen angle the radius x_0 can be varied within a range. From the definition of $I(\mathbf{k}, t)$ the expectation value of the effective magnetic field can be calculated:

$$\langle B(t) \rangle = \frac{I_0}{(\alpha)^3} \sqrt{\frac{1}{A^3}} e^{-x_0^2/A}, \quad (25)$$

where we have defined $A = \alpha^{-2} + \beta^{-2} + 4Dt$. We are interested in the correlation function for the magnetic field $\langle B(t+s)B(s) \rangle$ which is calculated to be

$$\begin{aligned} \langle B(t+s)B(s) \rangle &= \frac{I_0^2 e^{-x_0^2/F_1} e^{-x_0^2/F_2}}{(\alpha)^6 \sqrt{F_1^3 F_2^3}} \\ &\quad - \frac{\eta}{2\pi^{3/2}} \left(\frac{1}{F_3^{3/2}} - \frac{1}{F_4^{3/2}} \right), \end{aligned} \quad (26)$$

where we have defined the following constants

$$F_1 = \alpha^{-2} + \beta^{-2} + 4D(t+2s), \quad (27)$$

$$F_2 = \alpha^{-2} + \beta^{-2}, \quad (28)$$

$$F_3 = 2\beta^{-2} + 4D(t+2s), \quad (29)$$

$$F_4 = 2\beta^{-2} + 4Dt. \quad (30)$$

Note that the additional time dependence due to ‘ s ’ in the above equations arises because the nuclear diffusive dynamics start from a non-trivial source term (which comes from the DNP solution) at time ‘ s ’. This specifically means that we are first driving the system from time 0 to time s , resulting in an initial DNP distribution as discussed earlier. The parameter α is therefore a function of driving time ($\alpha = \alpha(s)$), as also demonstrated in Fig. 4. We now define the two point correlation function

$$C(t) = \langle B(s+t)B(s) \rangle - \langle B(s+t) \rangle \langle B(s) \rangle, \quad (31)$$

where the effect of the overall increase of the effective magnetic field $\langle B \rangle$ with the driving time has been removed by subtracting the mean value of the effective magnetic field. We point out that the Gaussian approximation allows us to analytically calculate the two point correlation function $C(t)$ in Eq. 31, which otherwise would not be feasible for a more

complex form of $I(\mathbf{x}, 0)$. The first spectral density is given by the Fourier transform of $C(t)$

$$C(\omega) = \int_{-\infty}^{+\infty} dt e^{-i\omega t} C(t). \quad (32)$$

Since the functional form of $C(t)$ given by Eqs. 31, 26, 25 does not allow an analytical expression for $C(\omega)$, we will resort to a numerical evaluation of the Fourier transform $C(\omega)$ in our calculations.

IV. ENHANCEMENT OF NUCLEAR COHERENCE TIME

In this section we will use the two point correlation function $C(\omega)$ to evaluate the coherence time T_2 . Let us consider the quantum state of a single nucleus prepared in an initial state $|\psi\rangle = c_\uparrow |\uparrow\rangle + c_\downarrow |\downarrow\rangle$ evolving under the stochastic field $B(t)$. The mean field $\langle B(t) \rangle$ and the correlation function of this field were obtained in the previous section (Eq. 25 and Eq. 26). The corresponding Hamiltonian is given by $H = \gamma_N B(t) \sigma_z / 2$, where σ_z is the Pauli matrix. The state at time t will be given by

$$|\psi(t)\rangle = e^{-\frac{i}{2} \int_0^t \gamma_N B(s) ds} c_\uparrow |\uparrow\rangle + e^{+\frac{i}{2} \int_0^t \gamma_N B(s) ds} c_\downarrow |\downarrow\rangle. \quad (33)$$

The off-diagonal element of the density matrix characterizes the nuclear coherence and can be quantified by the function $W(t)$ as:

$$W(t) = \frac{|\langle \rho_{\uparrow\downarrow}(t) \rangle|}{|\langle \rho_{\uparrow\downarrow}(0) \rangle|} = |\langle \exp(-i \int_0^t \gamma_N B(s) ds) \rangle|. \quad (34)$$

The function $W(t)$ in the above expression can describe decoherence effects corresponding to a free induction decay, i.e., the nucleus is prepared in a quantum state and allowed to evolve freely under the given Hamiltonian. For more complex pulse sequences (like spin echo, CPMG, CDD etc), a corresponding function $f(t, s)$ can be introduced in the integrand of the above equation to account for multiple pulses⁵⁴. The characteristic time of decay of $W(t)$ is denoted as T_2 , defined by $\log(W(T_2)) = -1$. Therefore one can typically write the relation $W(t) \equiv e^{-\chi(t)}$, where the quantity $\chi(t)$ can be written as⁵⁴

$$\chi(t) = \int_0^\infty \frac{d\omega}{2\pi} C(\omega) \frac{F(\omega t)}{\omega^2}, \quad (35)$$

where $C(\omega)$ is the first spectral density defined in Sec III Eq. 32. The function $F(z)$ is the filter function, which depends on the type of pulse sequence employed. It encapsulates the effect of the pulse sequence on decoherence. For example, the filter functions for spin echo (SE) and CPMG pulses are⁵⁴

$$F(z) = 8 \sin^4(z/4); \text{ for SE} \quad (36)$$

$$F(z) = 8 \sin^4(z/4n) \sin^2(z/2) / \cos^2(z/2n);$$

for CPMG even n. (37)

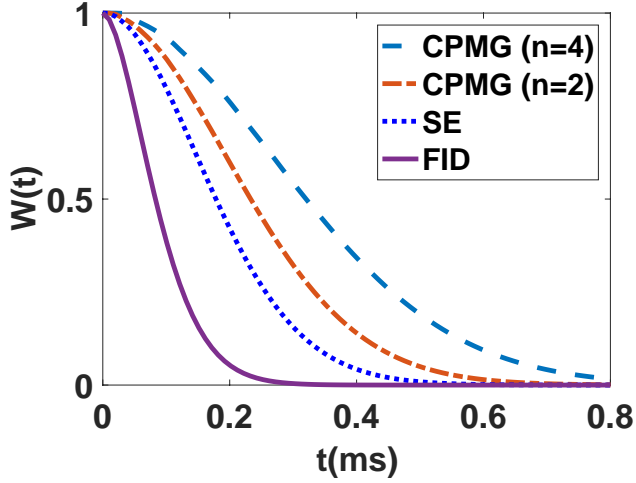


FIG. 5. Decoherence under various dynamical decoupling pulse sequences (free induction decay, spin echo and CPMG) for a driving time of $T \sim 0.01$ s. The other parameters used are $a_1 = -0.16632$, $a_2 = 18.8096$, $x_0 = 10$ nm, $D = 25$ nm²/s, $\beta^{-1} = 1$ Å, $\eta \sim 10^{-20}$ (eVs)²/m³, $I_0 = \sqrt{\pi\hbar}/(0.2\mu\text{m}^3)$.

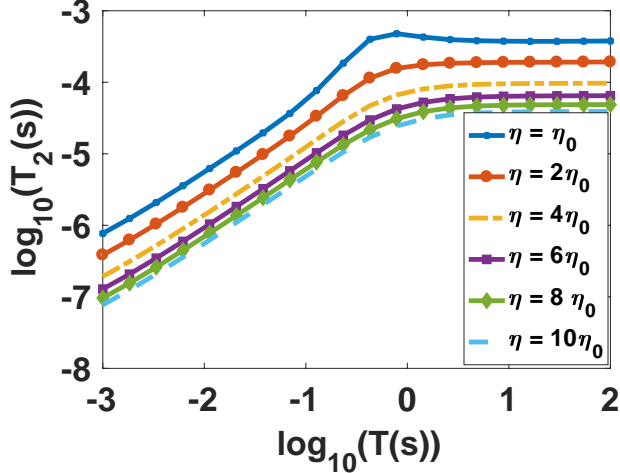


FIG. 6. Logarithm of the nuclear T_2 time as a function of the logarithm of the driving time for various different values of the noise strength η . A clear enhancement (up to ~ 3 orders of magnitude) of the nuclear T_2 time with driving time is seen for $-3 < \log_{10}(T) < 0$. We also note the suppression of T_2 time with increasing noise strength. Further the T_2 time saturates after the DNP drive time is increased beyond $T \sim 1$ s. We use $a_1 = -0.16632$, $a_2 = 18.8096$, $x_0 = 10$ nm, $D = 25$ nm²/s, $\eta_0 \sim 10^{-20}$ (eVs)²/m³, $\beta^{-1} = 1$ Å, and use the $n = 4$ CPMG pulse sequence.

Fig. 5 shows decoherence under free induction decay and various dynamical decoupling pulse sequences (Hahn's spin echo and CPMG pulses) for a chosen driving time of $T \sim 0.01$ s. As one would expect, the dephasing slows down as more dynamical decoupling pulses are applied. In Fig. 6 we show the logarithm of the nuclear T_2 as a function of the logarithm of the driving time for various values of the stochastic noise pa-

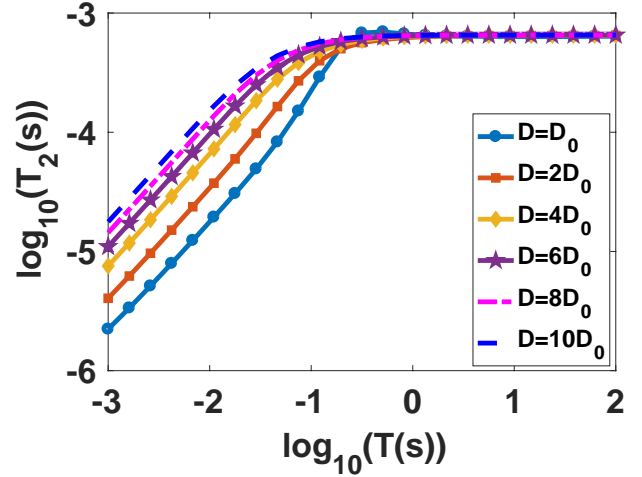


FIG. 7. Logarithm of the nuclear T_2 time as a function of the logarithm of the driving time for various different values of the diffusion constant D . For larger D values the coherence time saturates more quickly as a function of driving time. We use $a_1 = -0.16632$, $a_2 = 18.8096$, $x_0 = 10$ nm, $\eta \sim 10^{-20}$ (eVs)²/m³, $\beta^{-1} = 1$ Å, $D_0 = 0.5$ nm²s⁻¹, and use the $n = 4$ CPMG pulse sequence.

rameter η . We see a clear enhancement of the nuclear T_2 time with driving time for $-3 < \log_{10}(T) < 0$. The T_2 time is suppressed with increasing noise parameter η , however we point out that it is essential that $\eta \neq 0$ in order to obtain physically acceptable results for T_2 . Further we also note that the T_2 time saturates after the driving time is increased beyond a certain time T_{sat} . The exact value of the obtained T_2 time and the saturation time depends on our choice of parameters. Fig. 7 shows the logarithm of the nuclear T_2 as a function of the logarithm of the driving time for various values of the diffusion constant D . We note that for a higher diffusion constant, the T_2 coherence time saturates more quickly as a function of driving time. This behavior is expected because a higher diffusion rate should increase the temporal spread of the driving induced polarization (see Eq. 12), however η sets the scale for an upper limit on T_2 . Fig. 8 shows the density plot for the nuclear T_2 time as a function of the noise strength and diffusion constant for a constant driving time T . We note that an increase in noise strength leads to a higher suppression of T_2 compared to lowering the diffusion constant D . The different order of the T_2 obtained in Fig. 8 is due to our different choice of parameters compared to Fig. 6 and Fig. 7.

The two processes that play a central role in our analysis are DNP induced by driving electron-nuclear flip-flops and noisy diffusion caused by nuclear dipole-dipole interactions. For finite magnetic fields the dipolar interaction between two nuclei can be effectively written as a sum of Overhauser and flip-flop terms $H_{dip} \approx t'(I_{+i}I_{-j} + I_{+j}I_{-i} - 2I_{zj}I_{zi})$, where t' is the energy scale of the interaction, and i, j represent nuclei indices. When the nuclear bath is completely unpolarized ($m = 0$), the distribution of the nuclear spins in the configuration space has the maximum entropy, while for a fully polarized nuclear bath ($m = 1$) the configurational entropy is

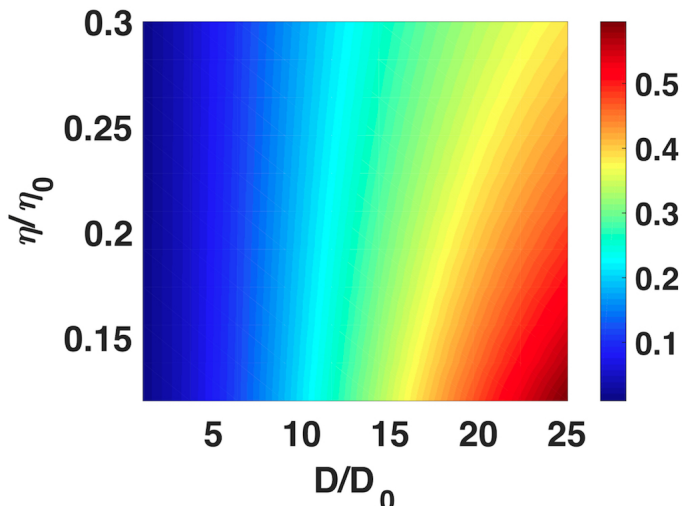


FIG. 8. Density plot for the nuclear T_2 time (in seconds) as a function of the noise parameter and diffusion constant for a constant driving time of $T = 10$ s. The parameters used were $D_0 = 25\text{nm}^2/\text{s}$, $\eta_0 \sim 10^{-23}(\text{eVs})^2/\text{m}^3$, $a_1 = -0.1662$, $a_2 = 18.4374$, $x_0 = 10\text{nm}$, $\beta^{-1} = 1\text{\AA}$, and the $n = 4$ CPMG pulse sequence was used. An increase in noise strength leads to a higher suppression of T_2 compared to lowering the diffusion constant D . The different order of the T_2 obtained here is due to our different choice of parameters compared to Fig. 6 and Fig. 7.

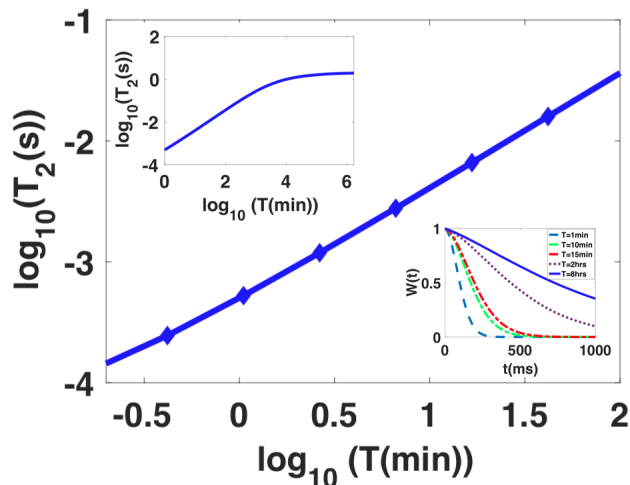


FIG. 9. Plot of the logarithm of the nuclear T_2 time as a function of logarithm of the DNP polarization time for experimentally relevant parameters for nanodiamond²⁸ i.e. $D = 5\text{nm}^2/\text{s}$, $\omega_{0s} \sim 300\mu\text{eV}$. Note that for this plot we perform the ensemble averaging to obtain the T_2 time over a wide range of radii from the center $0.5\text{nm} < x_0 < 10\text{nm}$ and also over the angle θ . For the DNP Gaussian model for each θ we have calculated α separately from the exact DNP solution. The top inset shows the saturation of the T_2 time for arbitrarily higher DNP driving times and the bottom inset shows the decay of the signal with time for increasing DNP driving times. The other parameters we chose $\beta^{-1} = 1\text{\AA}$, $\eta \sim 10^{-23}(\text{eVs})^2/\text{m}^3$ ⁴⁶, and the $n = 4$ CPMG pulse sequence.

zero as there is only one way to arrange the spins. Therefore when we consider processes in which the total spin is conserved, such as a pair of spin-flips which causes fluctuations in the magnetic field (noise), an unpolarized bath is expected to result in maximal noise and therefore the lowest coherence time T_2 , while a fully polarized bath should result in minimal noise and a maximal (ideally infinite if other decoherence processes are ignored) T_2 time. For intermediate bath polarizations, the phase space for flip-flops is reduced and is sharply peaked around $m = 0$. Therefore physically we also expect that longer driving times, which causes higher average bath polarization, should result in an enhanced T_2 coherence time. Further we note that all the curves in Fig. 7 saturate to the same value of T_2 indicating the fact that the nuclear polarization itself saturates to the same distribution regardless of the diffusion constant. The magnitude of the diffusion constant only affects how quickly the DNP reaches its saturation value. The T_2 time for a nucleus at $x = 10\text{nm}$ only improves once the DNP has propagated till x_0 from the electron defect center, after which the T_2 time remains a constant as the DNP wave continues to propagate outwards, and the DNP becomes uniform over the sample.

In Fig. 5- 8 we demonstrated the generic behavior of the T_2 time as a function of the driving time as obtained within our theoretical model. In actual hyperpolarization experiments, the driving time can be increased up to a few minutes or even hours. In recent experiments²⁸ performed on nanodiamond, an increase of the relaxation time of ^{13}C spins up to 3 orders of magnitude has been observed by dynamically hyperpolarizing the nuclear bath via microwave driving. In Fig. 9 we plot the T_2 coherence time using experimentally relevant parameters for nanodiamond and note that the nuclear coherence time increases up to 3 orders of magnitude ($\sim 1\text{ms}$ - 1s) as the driving time is increased. Note that for this plot we perform the ensemble averaging to obtain the T_2 time over a wide range of radii from the center $0.5\text{nm} < x_0 < 10\text{nm}$ for a particular θ and also average over the angle θ . Since the DNP solution is anisotropic and has a C_4 symmetry, for the Gaussian model for each θ we have calculated α separately from the exact DNP solution. Our theoretical results suggest that nuclear hyperpolarization via microwave driving not only enhances relaxation times but also nuclear spin coherence times by several orders of magnitude.

V. CONCLUSION

In this work, we calculated the nuclear spin coherence time for an ensemble of dipolar-coupled nuclear spins in the vicinity of a driven defect center in a solid. We showed that when electron-nuclear spin-flip transitions are driven with microwave fields, nonsecular terms in the electron-nuclear hyperfine interaction can generate a large dynamic nuclear polarization. We calculated the spatial distribution of this polarization as a function of the driving time and used this as a starting point to study the subsequent diffusion and fluctuations of the polarization. Using these results, we then obtained the coherence times of nuclear spins far from the defect cen-

ter as a function of the driving time, fluctuation strength, and speed of diffusion. We found that the coherence generically increases by several orders of magnitude as the driving time is increased up until a saturation point that depends on the strength of the dipolar interaction. In the case of ^{13}C nuclear spins, this translates to a nearly three orders of magnitude coherence time increase, a result that parallels a similar enhance-

ment in relaxation times seen in recent experiments²⁸. Our theoretical model and results will be therefore useful for current and upcoming experiments on enhancing the coherence time via DNP.

Acknowledgment: The work of E.B. and S. E. was supported by NSF (Grant No. 1741656).

- ¹ J. J. Pla, K. Y. Tan, J. P. Dehollain, W. H. Lim, J. J. Morton, D. N. Jamieson, A. S. Dzurak, A. Morello, *Nature* **489**, 541 (2012).
- ² S. Thiele, F. Balestro, R. Ballou, S. Klyatskaya, M. Ruben, W. Wernsdorfer, *Science* **344**, 1135 (2014).
- ³ A. M. Tyryshkin, S. A. Lyon, A. V. Astashkin, A. M. Raitsimring, *Phys. Rev. B* **68**, 193207 (2003).
- ⁴ F. Jelezko, T. Gaebel, I. Popa, M. Domhan, A. Gruber, J. Wrachtrup, *Phys. Rev. Lett.* **93**, 130501 (2004).
- ⁵ F. Jelezko, T. Gaebel, I. Popa, A. Gruber, J. Wrachtrup, *Phys. Rev. Lett.* **92**, 076401 (2004).
- ⁶ S. A. Wolf, D. D. Awschalom, R. A. Buhrman, J. M. Daughton, S. Von Molnar, M. L. Roukes, A. Y. Chtchelkanova, D. M. Treger, *Science*. **294**, 1488 (2001).
- ⁷ Y. Ohno, D. K. Young, B. A. Beschoten, F. Matsukura, H. Ohno, D. D. Awschalom, *Nature* **402**, 790 (1999).
- ⁸ A. Imamog, D. D. Awschalom, G. Burkard, D. P. DiVincenzo, D. Loss, M. Sherwin, A. Small, *Phys. Rev. Lett.* **83**, 4204 (1999).
- ⁹ D. D. Awschalom, M. E. Flatte, *Nature Physics* **3**, 153 (2007).
- ¹⁰ D. D. Awschalom, D. Loss, N. Samarth, N. *Semiconductor spintronics and quantum computation*, Springer Science & Business Media; (2013).
- ¹¹ T. Van der Sar, Z. H. Wang, M. S. Blok, H. Bernien, T. H. Taminiu, D. M. Toyli, D. A. Lidar, D. D. Awschalom, R. Hanson, V. V. Dobrovitski, *Nature* **484**, 82 (2012).
- ¹² A. G. Curto, G. Volpe, T. H. Taminiu, M. P. Kreuzer, R. Quidant, N. F. van Hulst, *Science* **329**, 930 (2010).
- ¹³ J. R. Maze, P. L. Stanwix, J. S. Hodges, S. Hong, J. M. Taylor, P. Cappellaro, L. Jiang, M. G. Dutt, E. Togan, A. S. Zibrov, A. Yacoby, *Nature* **455**, 644 (2008).
- ¹⁴ P. L. Stanwix, L. M. Pham, J. R. Maze, D. Le Sage, T. K. Yeung, P. Cappellaro, P. R. Hemmer, A. Yacoby, M. D. Lukin, R. L. Walsworth, *Phys. Rev. B* **82**, 201201 (2010).
- ¹⁵ P. Maletinsky, S. Hong, M. S. Grinolds, B. Hausmann, M. D. Lukin, R. L. Walsworth, M. Loncar, A. Yacoby, *Nature nanotechnology* **7**, 320 (2012).
- ¹⁶ A. Abragam, M. Goldman, *Reports on Progress in Physics* **41**, 395 (1978).
- ¹⁷ A. W. Overhauser, *Phys. Rev.* **92**, 411 (1953).
- ¹⁸ J. Scheuer, I. Schwartz, Q. Chen, D. S-Sunninghausen, P. Carl, P. Hofer, A. Retzker, H. Sumiya, J. Isoya, B. Luy, M. B. Plenio, B. Naydenov, F. Jelezko, *New J. Phys.* **18**, 013040 (2016).
- ¹⁹ C. von Morze, R. A. Bok, G. D. Reed, J. H. Alarsen, J. Kurhanewicz, and D. B. Vigneron, *Magnetic resonance in medicine*, **72**, 1599 (2014).
- ²⁰ S. A. Sukhenko, and K.M. Salikhov, *Chemical Physics*, **98**, 431 (1985).
- ²¹ K. Tateishi, M. Negoro, S. Nishida, A. Kagawa, Y. Morita, and M. Kitagawa, *Proceedings of the National Academy of Sciences* **201315778** (2014).
- ²² P. London, J. Scheuer, J-M. Cai, I. Schwarz, A. Retzker, Martin B. Plenio, M. Katagiri, T. Teraji, S. Koizumi, J. Isoya, and R. Fischer, *Phys. Rev. Lett.* **111**, 067601 (2013).
- ²³ G. A. Alvarez, C. O. Bretschneider, R. Fischer, P. London, H. Kanda, S. Onoda, J. Isoya, D. Gershoni, and L. Frydman, *Nat. Comm.* **6**, 8456 (2015).
- ²⁴ P. Wang, and Q. Zheng, *The European Physical Journal D* **70**, 210 (2016).
- ²⁵ J. P. King, P. J. Coles, and J. A. Reimer, *Phys. Rev. B* **81**, 073201 (2010).
- ²⁶ Q. Chen, I. Schwarz, F. Jelezko, A. Retzker, and M. B. Plenio, *Phys. Rev. B* **92**, 184420 (2015).
- ²⁷ H. J. Wang, C. S. Shin, C. E. Avalos, S. J. Seltzer, D. Budker, A. Pines, and V. S. Bajaj, *Nat. Comm.* **4** 1940 (2013).
- ²⁸ E. Rej, T. Gaebel, T. Boele, D. E. J. Waddington, D. J. Reilly, *Nature communications* **6**, 8459 (2015).
- ²⁹ D. E. Waddington, M. Sarracanie, H. Zhang, N. Salameh, D. R. Glenn, E. Rej, T. Gaebel, T. Boele, R. L. Walsworth, D. J. Reilly, M. S. Rosen MS, *Nat. Comm.* **8**, 15118 (2017).
- ³⁰ C.P. Slichter, *Principles of Magnetic Resonance* (Springer-Verlag, Berlin, 1990).
- ³¹ L.J. Sham, *Journal of Magnetism and Magnetic Materials* **200**, 219 (1999).
- ³² U. Haeberlen, *High Resolution NMR in Solids, Advances in Magnetic Resonance Series, Supplement 1* (Academic, New York 1976).
- ³³ L. M. K. Vandersypen and I. L. Chuang, *Rev. Mod. Phys.* **76**, 1037 (2004).
- ³⁴ L. Viola and S. Lloyd, *Phys. Rev. A* **58**, 2733 (1998).
- ³⁵ L. Viola, *J. Mod. Opt.* **51**, 2357 (2004).
- ³⁶ P. Chen, *Phys. Rev. A* **75**, 062301 (2007).
- ³⁷ K. Khodjasteh and D. A. Lidar, *Phys. Rev. Lett.* **95**, 180501 (2005); *Phys. Rev. A* **75**, 062310 (2007).
- ³⁸ G. S. Uhrig, *Phys. Rev. Lett.* **98**, 100504 (2007).
- ³⁹ B. Lee, W. M. Witzel, and S. Das Sarma, *Phys. Rev. Lett.* **100**, 160505 (2008).
- ⁴⁰ D. J. Reilly, J. M. Taylor, J. R. Petta, C. M. Marcus, M. P. Hanson, and A. C. Gossard, *Science* **321**, 817 (2008).
- ⁴¹ S. Foletti, H. Bluhm, D. Mahalu, V. Umansky, and A. Yacoby, *Nat. Phys.* **5**, 903 (2009).
- ⁴² H. Bluhm, S. Foletti, D. Mahalu, V. Umansky, and A. Yacoby, *Phys. Rev. Lett.* **105**, 216803 (2010).
- ⁴³ E. Barnes, Edwin, L. Cywinski, and S. Das Sarma, *Phys. Rev. Lett.* **109**, 140403 (2012).
- ⁴⁴ I. J. Lowe and S. Gade, *Phys. Rev.* **156**, 817 (1967).
- ⁴⁵ D. Paget, *Phys. Rev. B* **25**, 4444 (1982).
- ⁴⁶ F. K. Malinowski, F. Martins, L. Cywinski, M. S. Rudner, P. D. Nissen, S. Fallahi, G. C. Gardner, M. J. Manfra, C. M. Marcus, and F. Kuemmeth, *Phys. Rev. Lett.* **118**, 177702 (2017).
- ⁴⁷ Z. X. Gong, Z. Q. Yin and L. M. Duan, *New Journal of Physics* **13**, 033036 (2011).
- ⁴⁸ J. P. Wolfe, *Phys. Rev. Lett.* **31**, 907 (1973).
- ⁴⁹ A. D. A. Hansen and J. P. Wolfe, *Phys. Lett.* **66**, 320 (1978).
- ⁵⁰ E. C. Reynhardt and G. L. High, *Journal of Chemical Physics* **109**, 4090 (1998).

- ⁵¹ M. J. R. Hoch and E. C. Reynhardt, Physical Review B **37**, 9222 (1988).
- ⁵² K. N. Hu, G. T. Debelouchina, A. A. Smith, R. G. Griffin, The Journal of chemical physics **134**, 03B622 (2011).
- ⁵³ P. C. Hohenberg, B. I. Halperin, Rev. Mod. Phys. **49**, 435 (1977).
- ⁵⁴ L. Cywinski, R. M. Lutchyn, C. P. Nave, S. D. Sarma, Phys. Rev. B **77**, 174509 (2008).